I J C T A, 9(32), 2016, pp. 79-92 ISSN: 0974-5572

Reduction of Stator Flux Ripples and Mitigation of Current Using Internal Model Control based Enhanced Field Oriented Control during Symmetrical Faults for Grid Connected DFIG at Different Loading Conditions

D.V.N. Ananth*[1] and G.V. Nagesh Kumar**

ABSTRACT

By adapting national grid codes, low voltage ride through issue and enhanced real and reactive power control with minimum penetration issues are most desired features of the latest wind turbine-generator system. In this paper, internal model control based enhanced field oriented control (EFOC) method is proposed for grid connected doubly fed induction generator (DFIG) to minimize torque pulsations, reduce rotor speed and current deviation and maintain nearly constant stator and rotor voltage and current during symmetrical grid fault by controlling the flux decay oscillations. The EFOC technique is adapted to the rotor side converter for DFIG than to grid side converter due to faster dynamic features and the reactive power capability of its rotor circuit. The system is analysed under three cases under symmetrical fault at point of common coupling with electro-magnetic torque of -10Nm, -20Nm and -30Nm.

Keywords: DFIG; field oriented control (FOC); internal model controller (IMC); low voltage fault ride through (LVRT); symmetrical faults

1. INTRODUCTION

The doubly fed induction generator (DFIG) is having better preference due to its low power ratings of converters, small size with higher MVA ratings available in the market, variable generator speed and constant frequency operation, robust four quadrant reactive power control and much better performance during the low voltage ride through (LVRT). However, such DFIG is sensitive to external disturbances like the voltage sag. If grid voltage falls suddenly due to any reason, large surge currents enter rotor terminals and voltage induces drastically. Hence, the rotor side converter (RSC) will get damaged due to exceeding voltage or the current rating. Apart from this, there will be huge electromagnetic torque pulsations and increase in rotor speed which may reduce gears of the wind turbine-generator lifetime. To ensure LVRT operation, crowbar protection [1-2], is used to bypass RSC during fault and surge current diverted to shunt electronic switch connected resistor, thereby protecting DFIG system.

Energy storage system like SMES, BESS and capacitor banks [3-5] and FACTS devices like STATCOM, DVR [6-9] and fault current limiters [10] are extensively used to enhance the performance of DFIG during

[1]* Dept. of Electrical & Electronics Engineering, DADI Institute of Engineering & Technology, Anakapalli, India, *Email: nagaananth@gmail.com*

[1] Corresponding author *Email: nagaananth@gmail.com*

** Dept. of Electrical & Electronics Engineering, GITAM University, Visakhapatnam, India.

faults. The techniques like feed-forward transient current control with PI [11] and PIR [12] are used, where stator and rotor current maintained nearly constant during symmetrical or asymmetrical faults. The LVRT issue with internal model control (IMC) with two degrees of freedom was explained in [13]. Further techniques for LVRT are available in [14-24] for better performance for LVRT issues.

In this paper, DFIG operation with the symmetrical grid fault under different loadings on the generator is analyzed. For a conventional system, Field Oriented Control (FOC) technique is most widely applied for a DFIG system due to many advantages as listed in literature, but, during grid fault conditions, FOC based DFIG performance degrades and gets to settle slowly after the fault was recovered. During fault, flux decay is not uniform and is with large oscillations, so electromagnetic torque also oscillates, speed of rotor increases with the decrease in flux, direct and quadrature (d and q) axis stator and rotor current changes and thereby voltages also changes. So, if flux decay is controlled, above all parameters of the machine can be easily controlled. For this Enhanced FOC called (EFOC) is proposed in which flux decay is controlled by using DC-offset flux control and flux trajectory radius control. The system performance is compared with PI and Internal Model Control (IMC) based current control technique with symmetrical grid fault conditions under three cases like EMT is -10Nm, -20Nm and -30Nm. The machine parameters under study are stator magnitude of flux, electromagnetic torque, speed of the rotor, stator and rotor currents.

2. MATHEMATICAL ANALYSIS OF RSC OF DFIG DURING STEADY STATE AND TRANSIENT STATE

The conventional demagnetization or field oriented control (FOC) scheme for DFIG is adopted in a synchronously rotating frame. It is to assist for decoupled active and reactive power management and to improve the system operation during transients with better dynamic response. The DFIG equivalent circuit [1], [2], [10] and [26], the dynamics of vectors are shown in GSC and RSC control schemes in Fig. 1 and 2. The external control loop for GSC derives relation with wind speed and mechanical power is done as per the table 1.

Table 1
Lookup table showing the relation of wind speed, rotor speed, mechanical power and output torque for certain speeds.

$V_{wind}(m/s)$	7	8	9	10	11	12	18
w_r (pu)	0.75	0.85	0.95	1.05	1.1	1.2	1.3
P_m (pu)	0.32	0.49	0.69	0.9	1	1.15	1.5
$T_m = \frac{P_m}{w_r}$ (pu)	0.48	0.58	0.73	0.85	0.9	0.95	1.15

2.1. Rotor Side Converter Control during steady state

RSC controller helps in improving reactive power demand at grid and to extract maximum power from the machine by making the rotor to run at optimal speed. The optimal speed of the rotor is decided from machine real power and rotor speed characteristic curves from MPPT algorithm. The stator active and reactive power control is possible with the RSC controller strategy through i_{qr} and i_{dr} components controlling respectively. The rotor voltage in a stationary reference frame and analysis from [23] is given by

$$V_r^s = V_{or}^s + R_r i_r^s + \sigma L_r \frac{di_r^s}{dt} - j\omega i_r^s \tag{1}$$

with $\sigma = 1 - \frac{L_{sm}^2}{L_s L_r}$ and ω_r is the rotor speed, i_r^s is the rotor current in a stationary frame of reference, L_s, L_r and L_m are stator, the rotor and mutual inductance parameters in Henry or in pu. V_{or}^s is initial rotor voltage in stationary frame. R_r is rotor resistance in ohms or in per-unit (pu).

The equation (1) in terms of rotor current and rotor flux can be written as

$$V_r^s = R_r i_r^s + \frac{d\phi_r^s}{dt} - j\omega_r \phi_r^s \tag{2}$$

From the basic equations of DFIG available in the literature, the equation (2) can be rewritten as

$$V_r^s = R_r i_r^s + \frac{d}{dt}\left(\frac{L_m}{L_s}\phi_s^s + \sigma L_r i_r\right) - j\omega_r\left(\frac{L_m}{L_s}\phi_s^s + \sigma L_r i_r\right) \tag{3}$$

Also, $\phi_s^s = \frac{V_s}{j\omega_s} e^{j\omega_s t}$ is the stator flux under normal conditions (4)

Rewriting the above equation (3), we get

$$V_r^s = (R_r i_r^s + \sigma L_r i_r \frac{di_r^s}{dt} - j\omega_r \sigma L_r i_r^s) + \left(\frac{L_m}{L_s}\frac{d\phi_s^s}{dt} - j\omega_r \frac{L_m}{L_s}\phi_s^s\right) \tag{5}$$

Substituting equation (4) in (5)

$$V_r^s = (R_r i_r^s + \sigma L_r i_r \frac{di_r^s}{dt} - j\omega_r \sigma L_r i_r^s) + \left(\frac{L_m}{L_s} s V_s^s e^{j\omega_{sr} t} - j\omega_r \frac{L_m}{L_s}\frac{V_s}{j\omega_s} e^{j\omega_s t}\right) \tag{6}$$

Here's' is slip speed, ω_{sr} is slip rotor speed and ω_s is synchronous speed of stator. In general the rotor speed ω_r is and the synchronous speed of stator is ω_s. But this synchronous frequency has to be changed from ω_s to a new synchronous speed value as described in flowchart later ω_s' as it is represented commonly by ω_1. Under ideal conditions, reference stator d-axis flux ϕ_d^* is zero and q-axis flux ϕ_q^* is equal to the magnitude of stator flux Φ_s for given back emf and rotor speed. The transient rotor dq axis current is given by equations (7A and 7B) as

$$\frac{di_{dr}}{dt} = -\frac{R_r}{\sigma L_r} i_{dr} + s\omega_s i_{qr} + \frac{1}{\sigma L_r} V_{dr} \tag{7A}$$

$$\frac{di_{qr}}{dt} = -\frac{-1}{\sigma}\left(\frac{R_r}{L_r} + \frac{R_s L_m^2}{L_s^2 L_r}\right) i_{qr} - s\omega_s i_{dr} + \frac{1}{\sigma L_r} V_{qr} \tag{7B}$$

The reference rotor voltages in dq transformation and from the control circuit are given below. This is the output voltage from rotor windings during normal and transient conditions.

$$V_{qr}^* = \left(i_{dr}^* + \frac{1}{\sigma}\left(\frac{R_r}{L_r} + \frac{R_s L_m^2}{L_s^2 L_r}\right) i_{qr} + s\omega_s i_{dr}\right)\sigma L_r \tag{8A}$$

$$V_{qr}^{*}=\left(i_{dr}^{*}+\frac{1}{\sigma}\left(\frac{R_r}{L_r}+\frac{R_s L_m^2}{L_s^2 L_r}\right)i_{qr}+s\omega_s i_{dr}\right)\sigma L_r \tag{8B}$$

The overall block diagram of the RSC is presented in Fig.1. The rotor speed is multiplied with pole numbers and is subtracted from angular grid synchronous frequency. Later integrated and given a 90º phase shift to get rotor slip injection frequency angles (θ_s). At this slip frequency RSC converter injects current into the rotor circuit to control the rotor speed for optimum value and to control grid reactive power. The stator voltage magnitude is compared and controlled using PI or IMC controller to get q-axis current. Similarly rotor actual speed and optimal speed reference are controlled using PI or IMC to get d-axis reference current. They are compared with an actual rotor d and q axis currents and controlled with tuned PI controllers to get the rotor injecting d and q axis voltages. The d and q voltages are converted into three axis abc voltage by using a Phase Locked Loop (PLL) with inverse Park's transformation and are given to a PWM pulse generator for getting pulses to RSC converter.

The equations 7A to 8B describe the design procedure for RSC and the necessity to control the rotor and voltage parameters. These equations are helpful in understanding the behavior of DFIG during and after the faults. The equation (4) describes the flux change during sudden transient and its exponential decay. The interaction between stator and rotor flux during the fault and control in the decay in stator flux understanding are important for effective operation during faults. The equations from 6 to 8B are back emf in the rotor during normal and transient conditions represented with equivalent diagram as in Fig. 2.

For better dynamic stability of grid connected DFIG, proposed method controls the decrease in the stator and rotor flux magnitude with control in decay in flux decomposition and damps power and torque oscillations during fault instances. To get better operation during disturbances, this paper adopts a strategy for rotor frequency reference to change to zero or other smaller value depending on the type and severity of the disturbance. This makes the phase locked loop of RSC to change its value during the fault, which makes the synchronization to stator voltage accordingly. This reduces the flux decay in stator and rotor windings effectively during faults. This ensures the dc offset components entering into the DFIG windings. Hence overall performance of grid connected DFIG is technically improved. The precise measurement

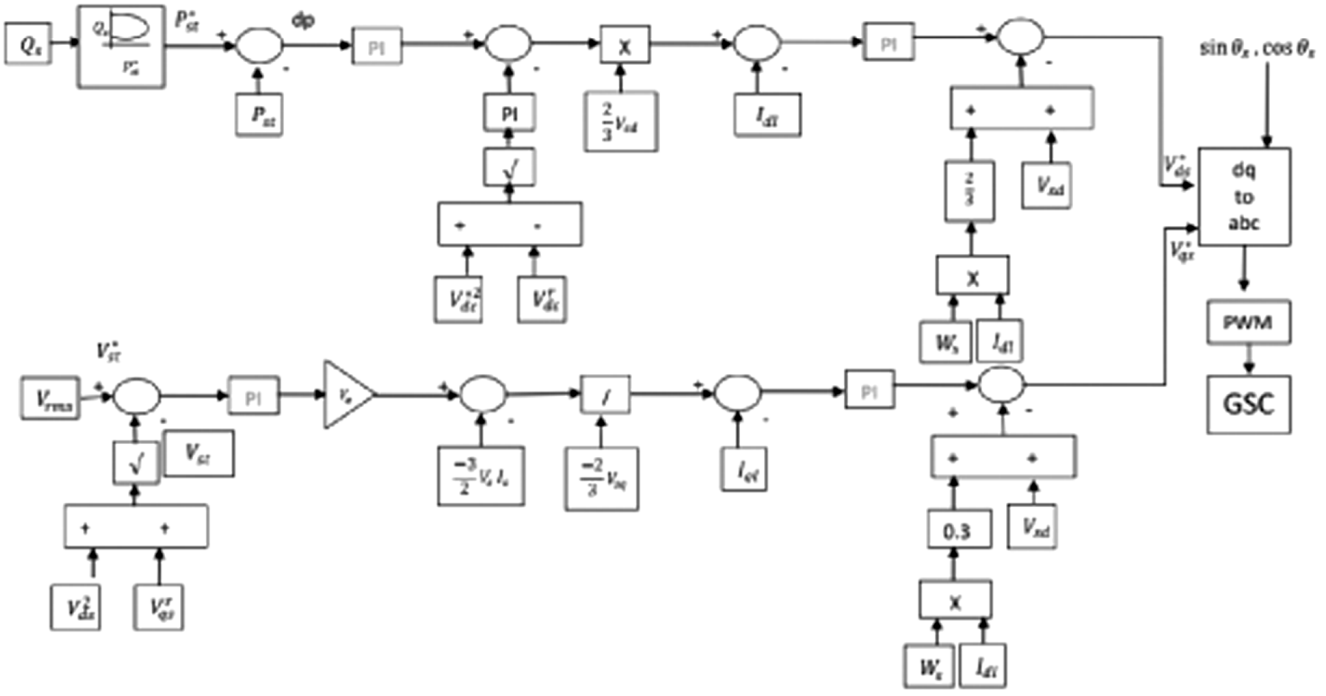

Figure 1: Block diagram of GSC controller design for Grid connected DFIG

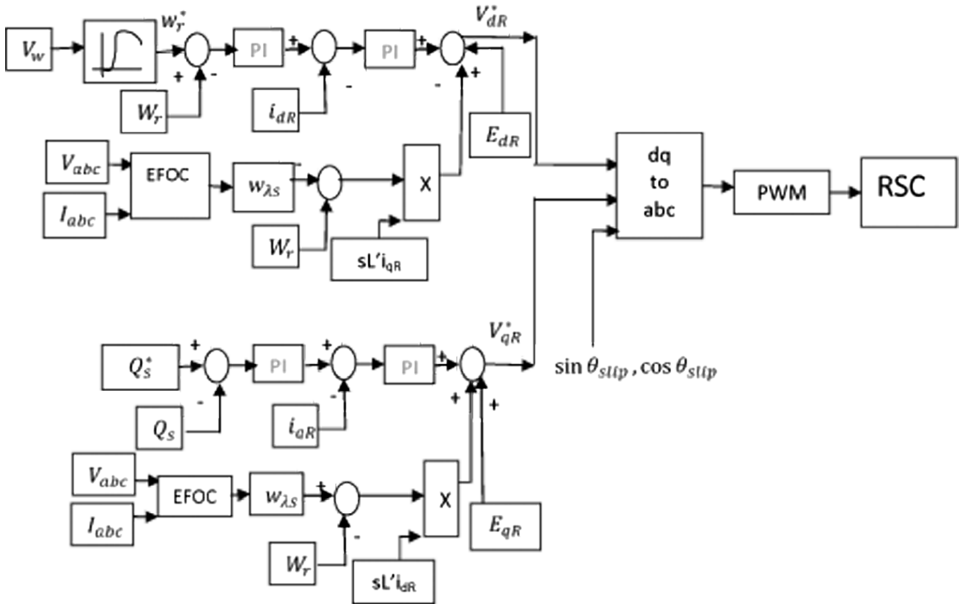

Figure 2: block diagram of the RSC controller with EFOC technique design for Grid connected DFIG

of stator and rotor parameters like flux, voltage, speed, angle and current helps in achieving better performance during disturbances. The reduction in dc offset stator current at transients and getting the two axis flux and voltage trajectories circular will improve the efficacy of the DFIG system during any faults. The equations 4 to 8 helps to understand the grid connected DFIG behavior during transient conditions and accuracy of its working depends on measurement of rotor current and flux parameters. The grid side controller (GSC) GSC control circuit block diagram is shown in Fig. 1 and of RSC for enhancing performance for LVRT issues is shown in Fig. 2. During normal conditions, the reactive power will be zero or very low and hence stator power pumped to grid will be high. This power control can done using the outer control loop of GSC.

In the same way generally stator voltage (V_s^*=1) or reference reactive power (Q_s^*=0), actual stator voltage Vs or reactive power Q_s is decreased by the PI controller and multiplied with the reactive power constant (K_q) for actual reference reactive power recompense parameter. From the equation (21), actual reactive power is designed and this difference and actual reactive power compensating terms and dividing with $2/3V_{sq}$, to get q-axis reference current (I_{qref}). The difference in I_{qref} and I_q is controlled using PI to get reference q-axis voltage. To improve the transient response quickly and to minimize steady state error decoupled q-axis voltage to be added. Both d and q axis voltage so obtained are converted to three axis 'abc' parameters with inverse Park's transformation and this voltage is given to the PWM controller for grid side controller pulse generation.

With the changes in wind speed, rotor speed will also change by shifting the gears position in the wind turbine. If rotor speed is made to operate at reference wind speed, maximum power can be extracted from wind turbine generator set. This will happen during normal state of operation, but during abnormal conditions like faults, rotor speed increases which may damage gears of wind turbine. Hence speed of DFIG rotor must be controlled. As explained in section 2A, if rotor side converter is operated, the performance of DFIG can be improved. With deviation in rotor speed, direct axis current of RSC changes and with demand in reactive power during faults or so, quadrature axis component of current changes. When a fault occurs, speed of rotor changes and hence rotor frequency also changes. If with this changed rotor frequency, current is injected into the windings of stator terminal of DFIG, flux decay or oscillations in stator terminal can be reduced. This will further reduce the dc offset components of stator as explained from eq (8) to (14).

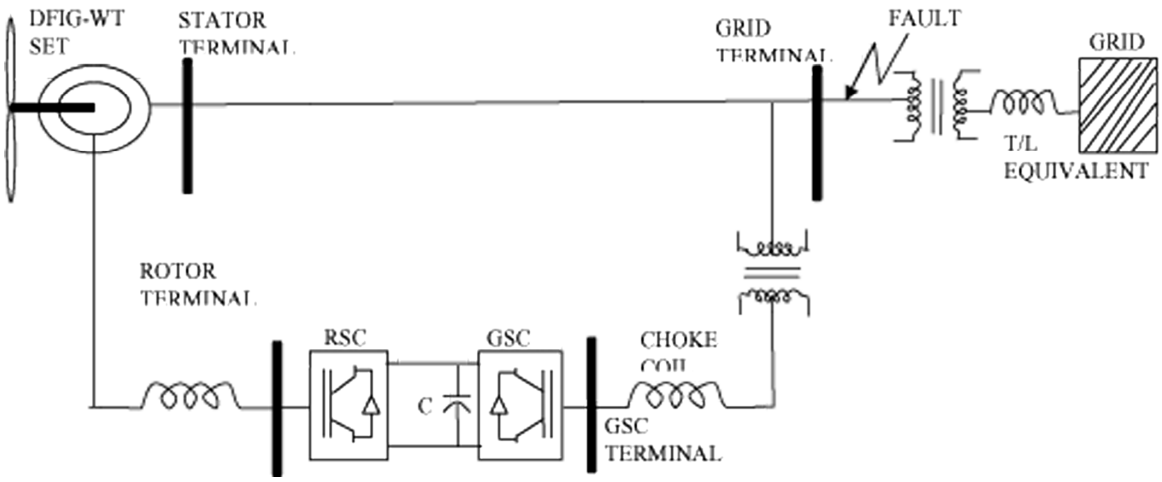

Figure 3: Grid connected DFIG showing the location of overvoltage fault

3. DESIGN OF INTERNAL MODEL CONTROLLER AND AN ENHANCED FOC (EFOC) CONTROLLER FOR LVRT ISSUE FOR DFIG

3.1. IMC controller technique

The mathematical modeling of IMC is given below

$$\omega_r' = \frac{K_t}{J_m} i_q - \frac{B\omega_r}{J_m} - \frac{T_L}{J_m} \tag{9A}$$

$$\omega_r' = \frac{K_t}{J_m} i_q^* - \frac{B\omega_r}{J_m} - \frac{K_t d(t)}{J_m} \tag{9B}$$

$$d(t) = \frac{-T_L}{K_t} - \left(i_q^* - i_q\right) \tag{10}$$

where w_r' is the differential rotor speed of DFIG, the speed controller block CIMC(s) is written as

$$\text{CIMC(s)} = \text{G(s) F(s)} \tag{11}$$

$$G(s) = \frac{1}{J's + B^1},$$

where J′ is $\frac{J}{K_t}$ and B′ is $\frac{B}{K_t}$, G(s) is the internal model block and F(s) is a filter component given by F(s) = $\frac{1}{Fs+1}$.Where F in the denominator is time constant for filter, ‘s’ is Laplace constant. The improved proposed IMC block diagram is shown in Fig. 4b and its implementation in MATLAB is shown in Fig. 4.

4. RESULTS AND DISCUSSION

In this grid connected DFIG behavior will be analyzed under three different loadings for DFIG during symmetrical fault at the grid during 2 to 3 seconds. The electromagnetic torque under three cases is: a) light load at -10Nm, b) medium load at -20Nm and c) full load at -30Nm. The analysis includes comparison of EFOC with conventional PI controller and IMC based technique. The generator torque rotor speed, stator

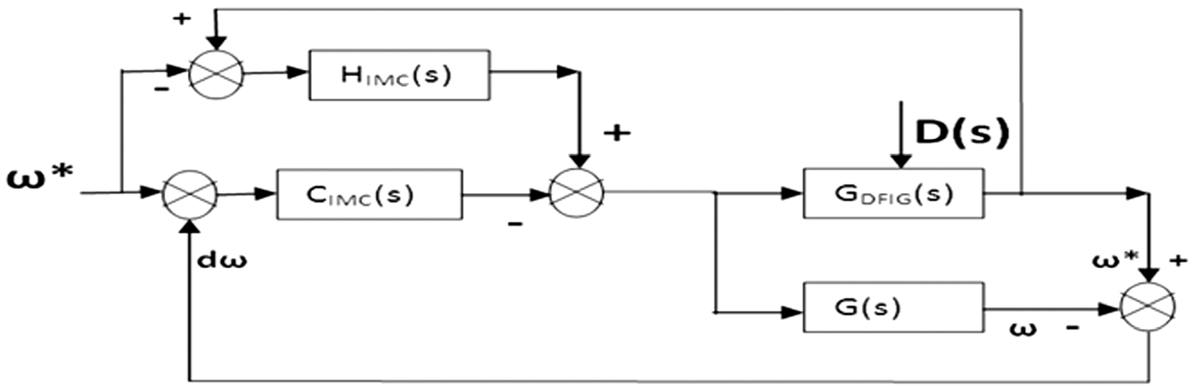

Figure 4: Improved IMC controller for DFIG

and rotor 3Φ current, rotor 2-axis current and stator flux were compared for finding the efficacy of the proposed system. The grid voltage before fault, during fault and after fault was reduced from 220 to 55 volts during 2 to 3 seconds. In all the three cases the same fault with the same voltage drop at the grid are considered and the results are presented.

4.1. Case a- EM Torque for DFIG is -10Nm

The EMT at 10Nm was considered in this case. A symmetrical severe fault occurs with voltage decreased from 220 volts per phase to neutral to 60V during 2 to 3 seconds. The stator flux magnitude dynamics with PI and IMC with EFOC technique was shown in Fig. 5a (i) and Fig. 5a (ii). It is observed that flux decay is from 0.6Wb to nearly 0.3Wb during fault with oscillations using the PI controller and reaching the steady state slowly. However, the flux decay with EFOC is less compared to conventional decoupled FOC technique. For the same system with IMC technique, the flux decay is also nearly same from 0.6Wb to 0.3Wb, but without oscillations and reaches a steady state very quickly. This the most efficient control of flux control with EFOC with an improved error control operation with IMC. It is observed that during severe grid fault, flux decay, elimination and maintaining constant flux is inevitable from the law of flux control action. With conventional technique, the flux decay reached 0.15Wb for the same system for the same fault (which is not shown here).

During this period, the EMT was dropped to nearly zero and after certain oscillations, reached to -10Nm even during fault with the PI controller as shown in Fig. 5b (i) and (ii). When fault was cleared, there is surge in torque and after certain oscillations, the system again sustained to pre-fault condition. With proposed EFOC technique with an IMC controller, there is surge impulse during and after fault instantly and oscillations were damped and faster steady state condition was achieved compared to PI control technique.

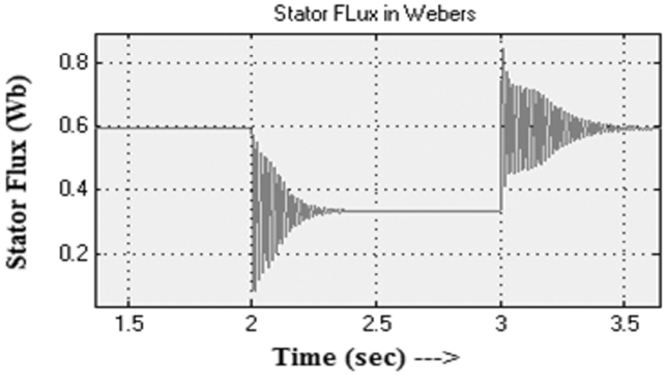

5a (i)

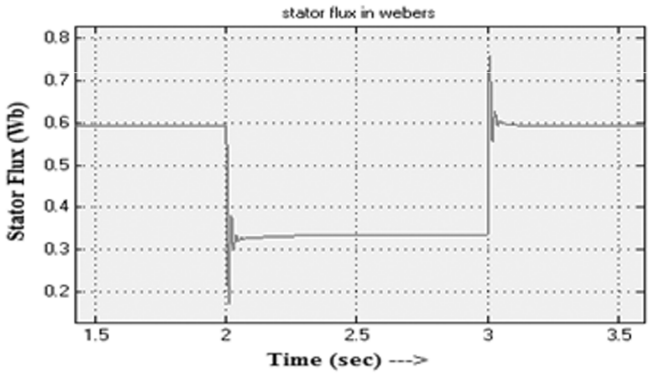

5a (ii)

Figure 5a: stator flux magnitude waveform with PI (i) and IMC (ii) EFOC technique at EMT=-10Nm

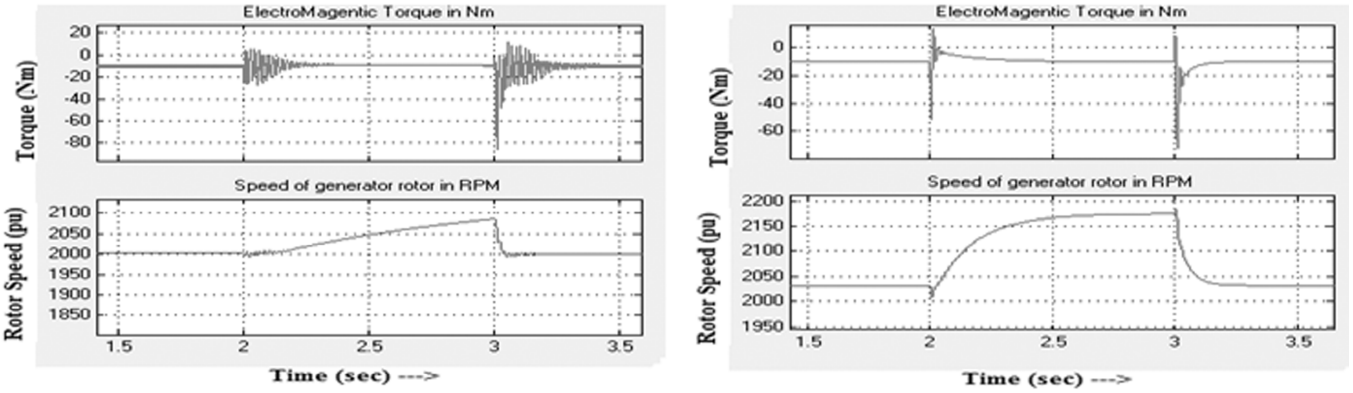

5b (i) 5b (ii)

Figure 5b: Electromagnetic torque and rotor speed with PI (i) and IMC (ii) EFOC technique at EMT=-10Nm

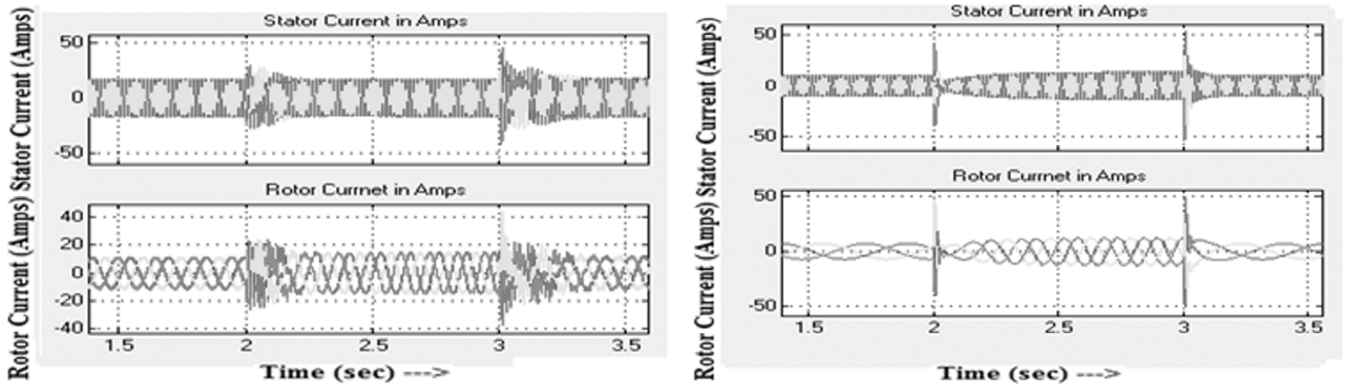

5c (i) 5c (ii)

Figure 5c: Stator and rotor three phase's waveform with PI (i) and IMC (ii) EFOC technique at EMT=-10Nm

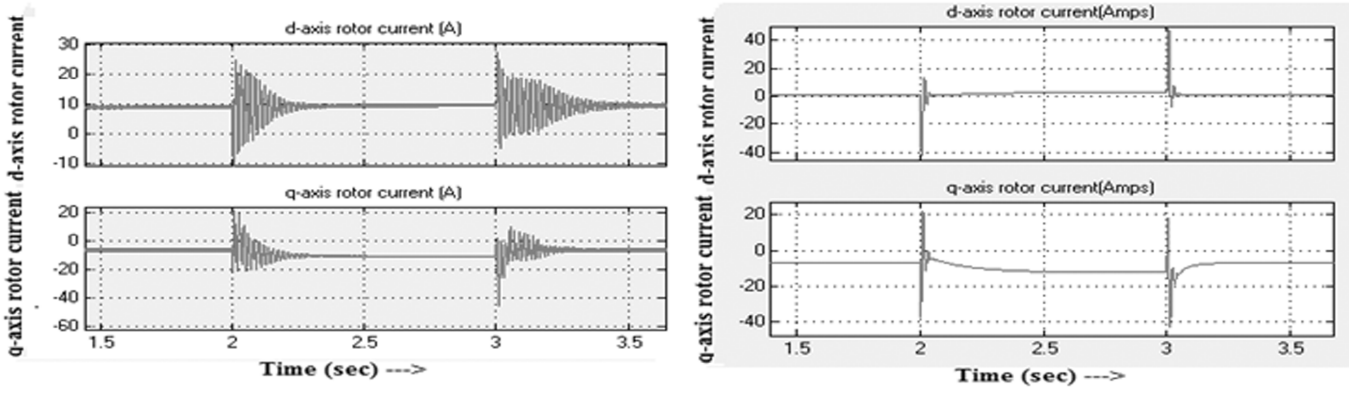

5d (i) 5d (ii)

Figure 5d: Rotor d and q axis current waveform with PI (i) and IMC (ii) EFOC technique ate EMT=-10NM

It is also be observed from Fig.5b that, there is a ramp type speed increment is observed with a conventional PI controller, whereas with proposed technique, rotor speed increased much greater than PI, but still maintaining constant speed. If fault was not cleared even after 3 seconds, rotor speed further increases and reaches a dangerously high value with the PI controller. However, with IMC technique, to any longer fault persists, rotor speed remains constant. This is due to maintaining the rotor flux decay with rotor q- axis current and voltage efficient control using EFOC and a faster dynamic action of IMC. In a conventional system without EFOC, torque of the generator reaches to zero value during fault and will attain the pre-fault state when the fault was relieved.

The stator and rotor three phases current with PI and IMC are sown in Fig. 5c. It is observed that with EFOC technique, stator and rotor current remained nearly constant with conventional PI Fig. 5c (i) and proposed IMC as in Fig.5c (ii). However, with IMC, few severe surges are observed in both current waveforms at the instant of fault occurrence and clearance, but with IMC, the rotor frequency remained constant throughout the fault, whereas with PI, the frequency increasing constantly during fault dynamics and later after fault clearance, in two cycles pre-fault state was achieved. IMC operation is faster than with a PI controller.

The direct (d) axis and quadrature (q) axis current of the rotor with the PI as in Fig. 5d (i) and IMC in Fig. 5d (ii) are shown in Fig. 5d. In this d-axis current changes from 10A to +25, -10A at the fault instant and after oscillations, the sinusoidal oscillations died out with PI based EFOC technique. Similarly, q-axis current also has oscillations with natural frequency from -10A to 20A and with oscillations died out slowly. In IMC based technique, d-axis rotor current is nearly zero before, during and after fault with surges at fault instants of ±40A is observed. The q-axis current is also nearly -10A during and after transients +20 A and -40A is observed.

5.2. Case b- EM Torque for DFIG is -20Nm

In this case, the EM Torque was increased from -10 to -20Nm with other parameters remaining same. The flux decay remained same but oscillations died early in this case with the PI controller as in Fig. 6a (i). The rate of change of flux depends on stator voltage and decoupled flux parameters. The higher the loading on the machine, more will be flux linking stator to the rotor, flux oscillations will be minimum. With IMC Fig. 6a (ii) also, flux decay is same, but without oscillations and is much stable than with PI controller in Fig. 6a (i) as shown in the Fig. 6a.

In this case, the EMT was dropped to nearly zero at the fault instant, and after certain oscillations, reached to -20Nm even during fault with PI controller as shown in Fig. 6b. At the fault clearing instant, there is surge in torque without oscillations from -20Nm to -250Nm with more than 12 times loading effect on it, but the system again sustained to pre-fault condition immediately in less than 0.2 seconds after fault clearance. With the proposed IMC controller, there is surge impulse during and after fault instantly and no oscillations is seen and faster steady state condition was achieved with IMC than compared to PI control technique. Also surge impulse after the fault clearance instant is only -100Nm than with -250Nm with PI technique.

It is observed from Fig.6b, the speed going on increasing from 200RPM to 2700RPM during fault and reaches to 2200RPM when fault was cleared with the PI controller as in Fig.6b (i), but with IMC as in Fig.6b (ii), the rotor speed increased from 2100RPM to 2400RPM during fault and maintained nearly

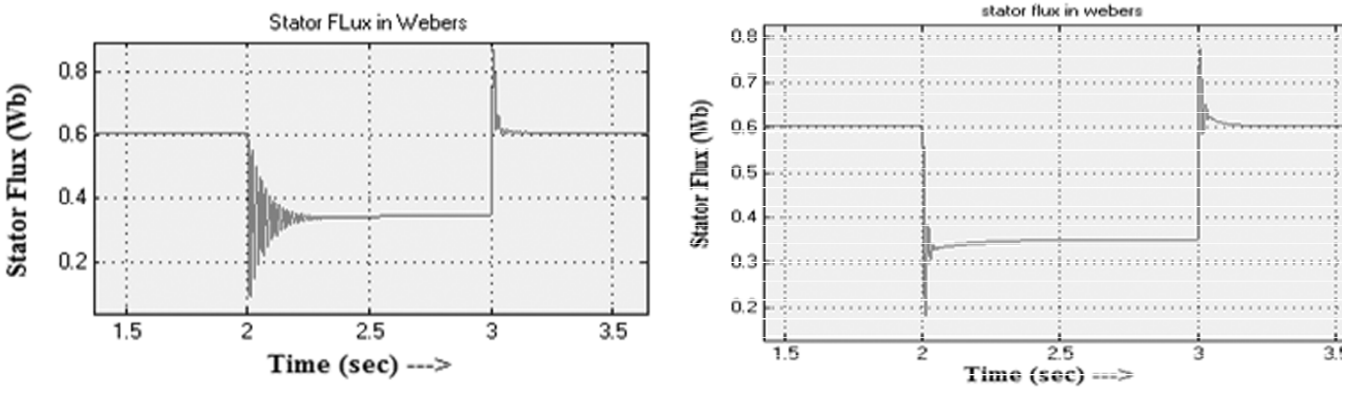

6a (i) 6a (ii)

Figure 6a: stator flux magnitude waveform with PI (i) and IMC (ii) EFOC technique at EMT=-20Nm

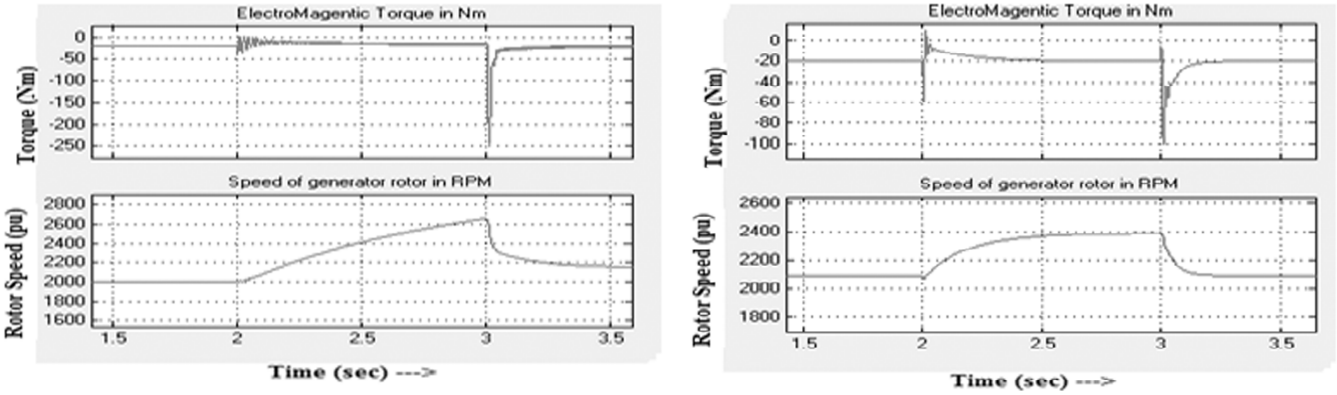

6b (i) 6b (ii)

Figure 6b: Electromagnetic torque and rotor speed with PI (i) and IMC (ii) EFOC technique at EMT=-20Nm

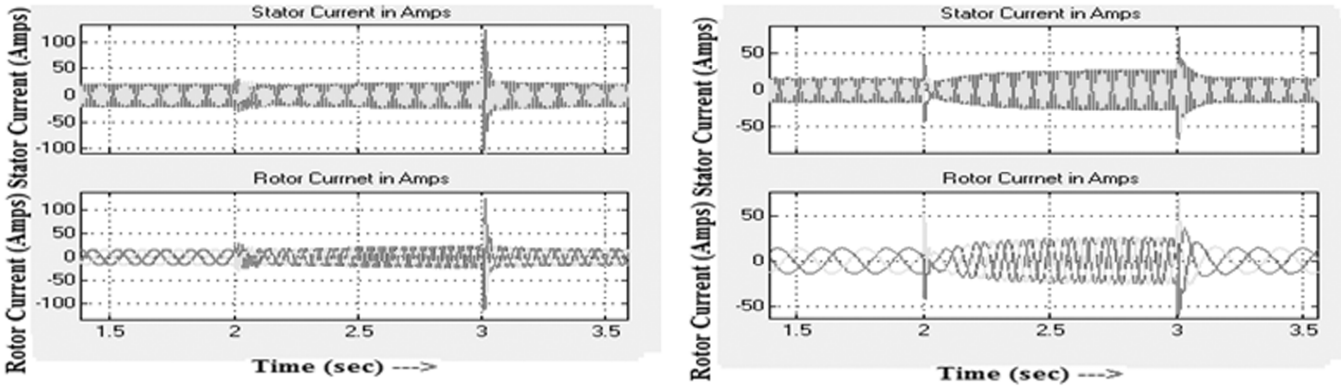

6c (i) 6c (ii)

Figure 6c: Stator and rotor the three phase's with PI (i) and IMC (ii) EFOC technique at EMT=-20Nm

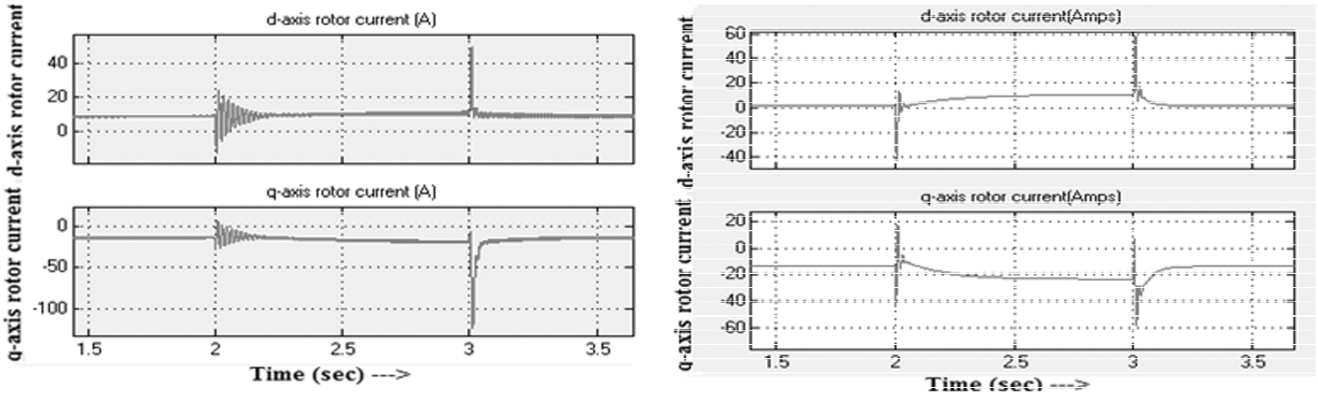

6d (i) 6d (ii)

Figure 6d: Rotor d and q axis current waveform with PI (i) and IMC (ii) EFOC technique ate EMT=-20NM

constant during fault and reaches pre-fault speed when the system was restored from fault. Hence, this method helps in maintaining flux; controlling rotor speed such that generator remains healthy during severe fault, as in Fig.6b. The stator and rotor current three phase's waveforms with PI in Fig.6c (i) and IMC in Fig.6c (ii) are shown in Fig.6c. It is observed that stator and rotor current were nearly constant in magnitude with the PI controller, but rotor frequency slowly increasing when fault started and surge current of 110A peak is observed in stator and rotor current waveforms.

Stator and rotor current magnitude increased during fault but rotor frequency increases and remained nearly constant, but surge current after faulty system recovery, is 60A on both stator and rotor side terminals

with IMC. The direct (d) axis and quadrature (q) axis current of the rotor with PI in Fig.6d (i) and IMC in Fig.6d (ii) are shown in Fig.6d. In this d-axis current changes from 10A to +50, -10A at this fault instant, and after oscillations, the sinusoidal oscillations died out with PI based EFOC technique. Similarly, q-axis current also has oscillations with natural frequency from -10A to 0 to -20A at fault occurrence instant and oscillations died out slowly. The post fault q-axis current reached to -130A from -16A as impulse current and reached to the steady state value very quickly with IMC than with PI controller.In IMC based technique, d-axis rotor current is nearly zero before fault, but during fault, direct axis current rose to 10A and after fault with surges at fault instants of +60 amps reaching the steady state quickly is observed. The q-axis current is also nearly -16A during and after transients +20A and -60A is observed which is less severe than the PI controller system.

5.3. Case C: EM Torque – 30Nm

In this case, the EM Torque was increased further from -20 to -30Nm with other parameters remaining same. The flux decay is from 0.6Wb to 0.38Wb during fault but oscillations died much early in this case with the PI controller as in Fig.7a (i). The rate of change of flux depends on stator voltage and decoupled flux parameters. The higher the loading on the machine, more will be flux linking stator to the rotor, flux oscillations will be minimum. With IMC in Fig.7a (ii) also, flux decay is same but without oscillations and is much stable than with the PI controller as shown in the Fig.7a.

In this case, the EMT was dropped to nearly zero as in Fig. 7b at the instant of a fault and after certain oscillations, reached to -30Nm even during fault with PI controller as in Fig.7b (i). At the fault clearing instant, there is surge in torque without oscillations from -30Nm to -270Nm with more than 9 times, loading effect on it, but the system again sustained to pre-fault condition immediately in less than 0.2 seconds after fault clearance. With the proposed IMC controller, there is surge impulse during and after fault instantly and no oscillations can be seen and faster steady state condition was achieved with IMC as in Fig.7b (ii) than compared to PI control technique. Also surge impulse after fault clearance instant is only -120Nm than with -270Nm with PI technique. It is observed from Fig.7b, the speed going on increasing from 210RPM to 2900RPM and remained constant during fault and reaches to 2350RPM when fault was cleared, but with IMC, the rotor speed increased from 2100RPM to 2600RPM during fault and maintained nearly constant during fault and reaches pre-fault speed when the system was restored from fault. Hence, this method helps in maintaining flux; controlling rotor speed such that generator remains healthy during severe fault.

The stator and rotor current waveforms with PI in Fig.7c (i) and IMC in Fig.7c (ii) are shown in Fig.7c. It is also observed that stator and rotor current were nearly constant in magnitude with the PI controller, but

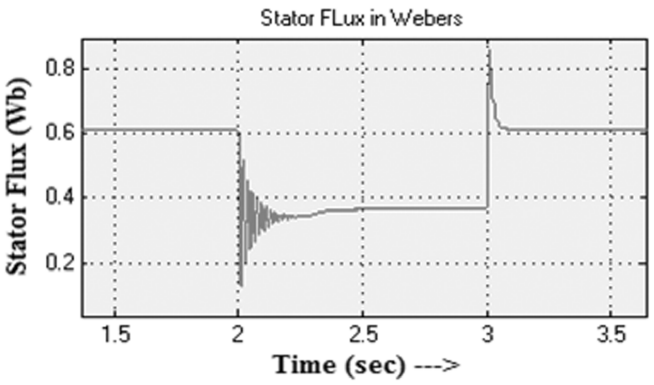

7a (i)

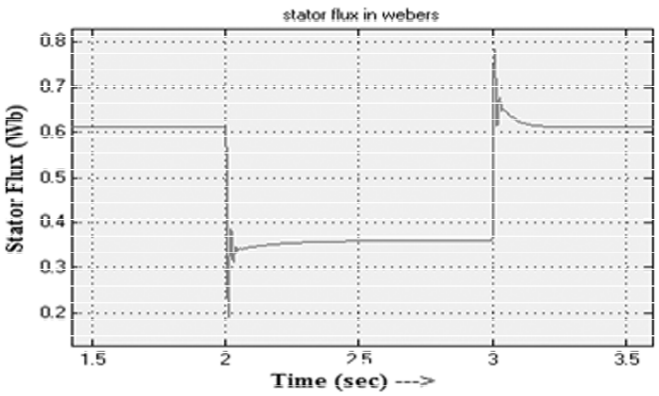

7a (ii)

Fig.7a stator flux magnitude waveform with PI (i) and IMC (ii) EFOC technique at EMT=-30Nm

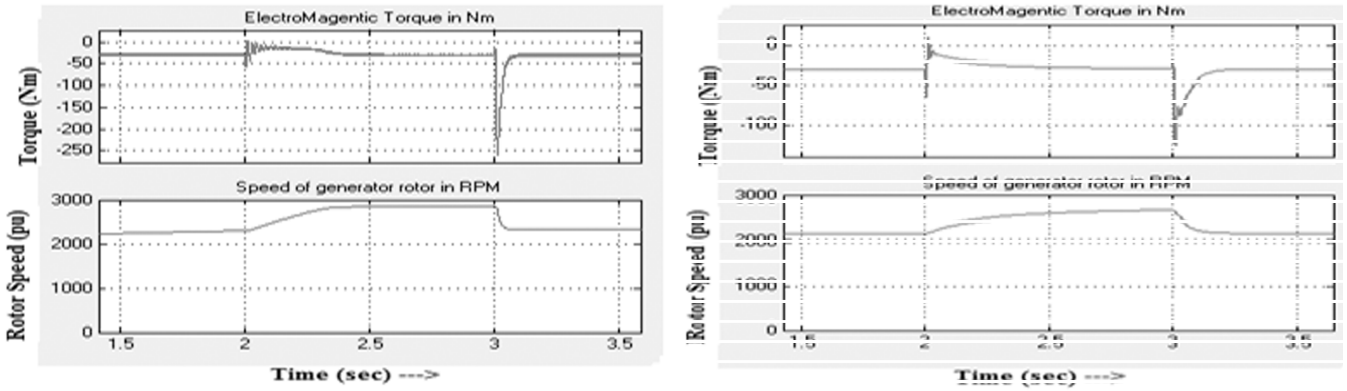

7b (i) 7b (ii)

Figure 7b: Electromagnetic torque and rotor speed with PI (i) and IMC (ii) EFOC technique at EMT=-30Nm

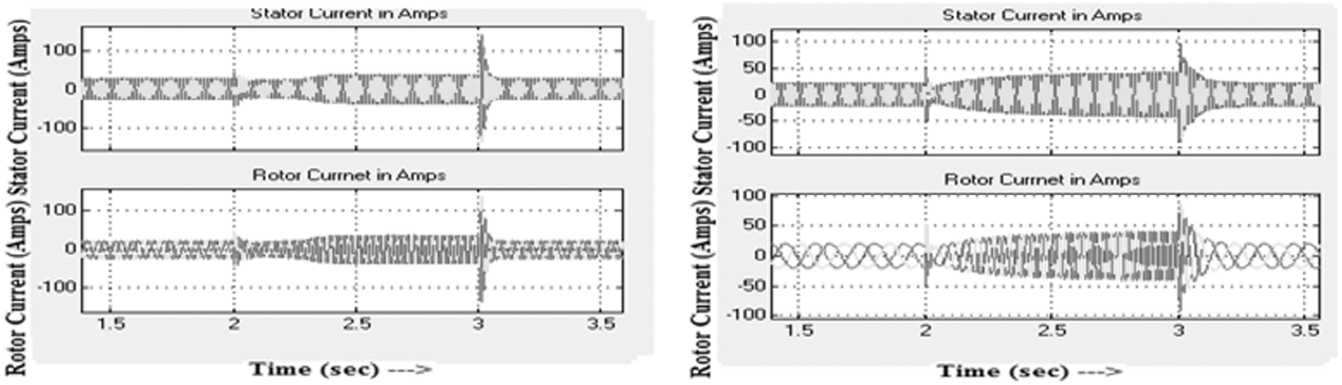

7c (i) 7c (ii)

Figure 7c: Stator and rotor three phase's current waveform with PI (i) and IMC (ii) EFOC technique at EMT=-30Nm

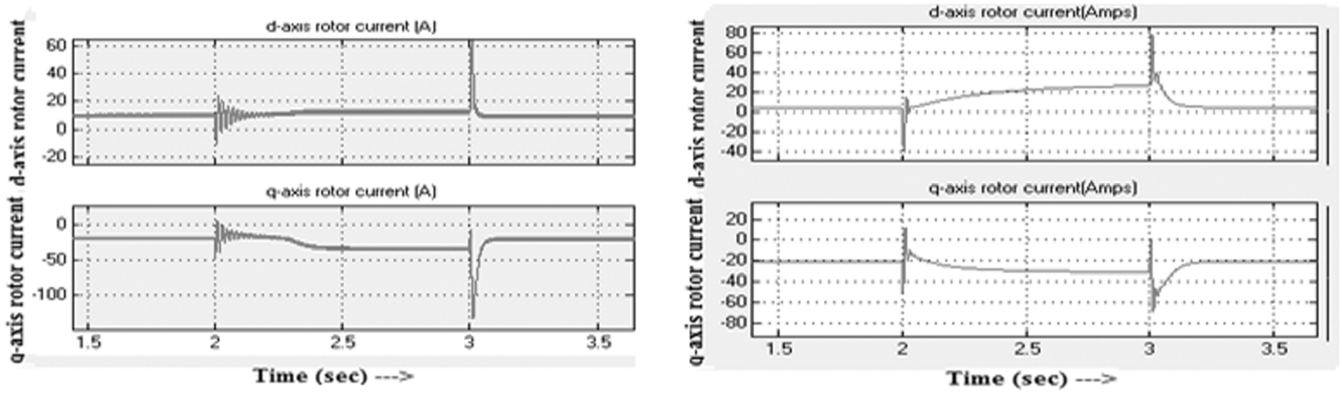

7d (i) 7d (ii)

Figure 7d: Rotor d and q axis current waveform with PI (i) and IMC (ii) EFOC technique ate EMT= -30NM

rotor frequency slowly increasing when fault started and surge current of 110A peak is observed in stator and rotor current waveforms. Stator and rotor current magnitude increased during fault but rotor frequency increases and remained nearly constant, but surge current after faulty system recovery, is 80A on both stator and rotor side terminals with IMC.

The direct (d) axis and quadrature (q) axis current of the rotor with PI in Fig.7d (i) and IMC in Fig.7d (ii) are shown in Fig.7d. In this d-axis current changes from 10A to +70A, -10A at the fault instant, and after oscillations, the sinusoidal oscillations died out with PI based EFOC technique. Similarly, q-axis current also has oscillations with natural frequency from -20A to 0 to -40A at the fault occurrence instant and

oscillations died out slowly. The post fault q-axis the current reached -6A to -130A as impulse and reached to the steady state very quickly.

In IMC based technique, d-axis rotor current is nearly zero before fault, but during fault, direct axis current rose to 10A and after fault with surges at fault instants of +80 reaches a steady state quickly is observed. The q-axis current is also nearly -20A during and after transients +10A and -70A is observed which is less severe than the PI controller system. Compared to the performances in reference papers [6, 7 and 11], the proposed method has good dynamic response, lesser torque surges and oscillations, good restoring capability during the fault and enhanced stability when fault is cleared. Hence proposed EFOC scheme has better dynamic and transient stability compared to the literature.

5. CONCLUSION

In the analysis, EFOC technique performance was compared with the PI and Internal model based controller scheme for a symmetrical grid fault during 2 to 3 seconds of the time period with grid voltage falling from 220 to 55 volts. The stator flux decay is nearly constant with increase or decrease in load, however, flux oscillations decreased with an increase in load due to mechanical stiffness from the prime-mover. With IMC technique, flux oscillations damped very quickly due to rapid control of d and q axis rotor currents. The ripples and oscillations in flux are reduced with IMC for every DFIG parameter compared to PI controller. The system regained to normal state even though fault still existing with both PI and IMC with EFGOC technique. This is due to the fact that dc offset components are reduced in the rotor windings, rotor and stator current control mechanism became fast with developed demagnetization based FOC technique. The rotor speed increase is also within limits when severe fault occurring and the generator is under full load conditions. The increase in fault current surges is around twotimes at fault occurring and relieving instances, but regained to its pre-fault value when the fault still exists. The increase in dynamic and transient response with decreased flux, torque and current oscillations are the contributions in the paper.

For the same fault, under light load conditions, rotor speed increasing slowly than under more loaded system with the PI controller. However, with IMC technique after certain time, rotor speed remained constant during the fault period. Compared to PI, IMC technique is having very less electromagnetic torque pulsations and the torque surges also got reduced. The stator and rotor surge currents at the beginning and end of the fault increasing with an increase in load. For the proposed EFOC technique system, with severe fault in the grid, the stator and rotor voltage still maintained nearly constant magnitude of current with very less deviation from pre-fault frequency. With IMC, getting to a steady state during the fault also is better than with the PI controller. The d-axis current is nearly zero and –axis current is equal to the magnitude of current was achieved with IMC.

With the proposed hybrid IMC based EFOC technique; the rotor speed increase at the duration of the fault is controlled and maintained to constant and stable value which enhances the gear mechanism lifetime of turbine-generator set. The electromagnetic torque surges, stator and rotor current surges were minimized with the proposed controller scheme.

REFERENCES

[1] L. G. Meegahapola, T. Littler, and D. Flynn, "Decoupled-DFIG fault ride through strategy for enhanced stability performance during grid faults,"*IEEE Trans. Sustain. Energy*, vol. 1, no. 3, pp. 152–162, Oct. 2010.

[2] G. Pannell, B. Zahawi, D.J. Atkinson, and P. Missailidis , "Evaluation of the Performance of a DC-Link Brake Chopper as a DFIG Low-Voltage Fault-Ride-Through Device," *IEEE Trans. Energy Convers.*, vol. 28, no. 3, pp. 535–542, Sep. 2013.

[3] C. Abbey and G. Joos, "Supercapacitor Energy Storage for Wind Energy Applications", *IEEE Trans. Ind. Appl.*, vol. 43, no. 3, pp.763-776,May/Jun 2007.

[4] W. Guo, L. Xiao, and S. Dai, "Enhancing low-voltage ride-through capability and smoothing output power of DFIG with a superconducting fault-current limiter–magnetic energy storage system," *IEEE Trans. Energy Convers*., vol. 27, no. 2, pp. 277–295, Jun. 2012.

[5] P. Huang, M. S. E. Moursi, W. Xiao, and J. L. Kirtley, "Novel fault ride-through configuration and transient management scheme for doubly fed induction generator ", *IEEE Trans. Energy Convers*, vol. 28, no. 1 , pp. 86–94, Mar. 201 3.

[6] A. O. Ibrahim, T. H. Nguyen, D. C. Lee, and S.-C. Kim, "A fault ride through technique of DFIG wind turbine systems using dynamic voltage restorers," *IEEE Trans. Energy Convers.*, vol. 12, no. 3, pp. 871–882, Sep. 2011.

[7] C. Wessels, F. Gebhardt, and F. W. Fuchs, "Fault ride-through of a DFIG wind turbine using a dynamic voltage restorer during symmetrical and asymmetrical grid faults," *IEEE Trans. Power Electron.*, vol. 26, no. 3, pp. 807–815, Mar. 2011.

[8] D. Deepak Chowdary and G.V.Nagesh Kumar, "Restoration of Single Phase Distribution System Voltage under Fault Conditions with DVR using Sliding Mode Control", Indian Journal of Science and Technology, October 2008, Volume 1, No: 5, Page(s): 1-5, Gandhi nagar, Adyar, Chennai, India.

[9] A. K. Adinbo, "On-grid doubly-fed induction generator wind turbine with nine-switch converter as grid side converter for low voltage ride-through," M.S. thesis, Elect. Comp. Eng., Tennessee Technol. Univ., Cookeville, USA, p. 410

[10] W.Guo, L.Xiao, and S.Dai, "Enhancing Low voltage ride through capability and smoothing output power of DFIG with superconducting fault-current limiter magnetic energy storage system," *IEEE Trans. Energy Convers.*, vol. 27, no. 2, pp. 277–285, jun. 2012.

[11] J. Liang, Wei Qiao and R. G. Harley, "Feedforward transient compensation control for Low Voltage Ride Through Enhancement of DFIG wind turbines," *IEEE Trans. Energy Convers.*, vol. 25, no. 3, pp. 836–843, Sep. 2010.

[12] J. Liang, D. F. Howard, J. A. Restrepo, and R. G. Harley, "Feedforward transient compensation control for DFIG wind turbines during both balanced and unbalanced grid disturbances," *IEEE Trans. Ind. Appl.*, vol. 49, no. 3, pp. 1452–1462, May/Jun. 201 3.

[13] D.C. Gaona, E.L.Moreno-Goytia, O. Anaya-Lara, "fault ride through improvement of DFIG-WT by integrating a Two-Degrees-of-Freedom Internal Model Control," *IEEE Trans. Ind. Electron.*, vol. 60, no. 3, pp. 1133–1145, Mar. 201 3

[14] J. P. da Costa, H. Pinheiro, T. Degner, and G. Arnold, "Robust controller for DFIGs of grid-connected wind turbines," *IEEE Trans. Ind. Electron.*, vol. 58, no. 9, pp. 4023–4038, Sep. 2011.

[15] S. Xiao, G. Yang, H. Zhou, and H. Geng, "An LVRT control strategy based on flux linkage tracking for DFIG-based WECS," *IEEE Trans. Ind.Electron.*, vol. 60, no. 7, pp. 2820–2832, Jul. 201 3.

[16] H. Geng, C. Liu, and G. Yang, "LVRT capability of DFIG-based WECS under asymmetrical grid fault condition," *IEEE Trans. Ind. Electron.*, vol. 60, no. 7, pp. 2495–2509, Jun. 201 3.

[17] S. Xiao, G. Yang, H. Zhou, and H. Geng, "Analysis of the control limit for rotor-side converter of doubly fed induction generator-based wind energy conversion system under various voltage dips," *IET Renew. Power Gen.*, vol. 7, no. 1 , pp. 71 –81 , Jan. 201 3.

[18] T. Long, S. Shao, P. Malliband, E. Abdi, and R. A. McMahon, "Crowbarless fault ride-though of the brushless doubly fed induction generator in a wind turbine under symmetrical voltage dips," *IEEE Trans. Ind. Electron.*, vol. 60, no. 7, pp. 2495–2509, Jun. 201 3.

[19] Li Yang, Z. Xu, J. Ostergaard, Z. Y. Dong, and K. P. Wong, "Advanced control strategy of DFIG wind turbines for power system fault ride through," *IEEE Trans. Power Syst.*, vol. 27, no. 2, pp. 713–722, May 2012.

[20] M. J. Hossain, T. K. Saha, N. Mithulananthan, and H. R. Pota, "Control strategies for augmenting LVRT capability of DFIGs in interconnected power system," *IEEE Trans. Ind. Electron.*, vol. 60, no. 7, pp. 2495–2509, Jun. 201 3.

[21] D. xie, Z. Xu, L. Yang, J. Ostergaard, Y. Xue, and K. P. Wong, "A comprehensive LVR control strategies for DFIG wind turbines with enhanced reactive power support," *IEEE Trans. Power Syst.*, vol. 28, no.3, pp. 3302-3310, 2013.

[22] S. Q. Bu, W. Du, H. F. Wang, S. Gao, "Power angle control of grid-connected doubly fed induction generator wind turbines for fault ride-through," *IET Renew. Power Gen.*, vol. 7, no. 1, pp. 18–27, Jan. 201 3.

[23] T. Thiringer, A. Petersson, T. Petru, "Grid disturbance response of wind turbines equipped with induction generator and doubly-fed induction generator," in *Proc. IEEE Power Eng. Soc. General Meeting*, 2003, vol. 3, pp. 1542–1547.

[24] D.V.N. Ananth, G.V. Nagesh Kumar, Fault ride-through enhancement using an enhanced field oriented control technique for converters of grid connected DFIG and STATCOM for different types of faults, ISA Transactions, Volume 62, May 2016, Pages 2-18.